Anatomical Labeling of the Circle of Willis using Maximum A Posteriori Probability Estimation

Hrvoje Bogunović*, *Member, IEEE*, José María Pozo, Rubén Cárdenes, Luis San Román, and
Alejandro F. Frangi, *Senior Member, IEEE*

Abstract—Anatomical labeling of the cerebral arteries forming the Circle of Willis (CoW) enables inter-subject comparison, which is required for geometric characterization and discovering risk factors associated with cerebrovascular pathologies. We present a method for automated anatomical labeling of the CoW by detecting its main bifurcations. The CoW is modeled as rooted attributed relational graph, with bifurcations as its vertices, whose attributes are characterized as points on a Riemannian manifold. The method is first trained on a set of pre-labeled examples, where it learns the variability of local bifurcation features as well as the variability in the topology. Then, the labeling of the target vasculature is obtained as maximum a posteriori probability (MAP) estimate where the likelihood of labeling individual bifurcations is regularized by the prior structural knowledge of the graph they span. The method was evaluated by cross-validation on 50 subjects, imaged with magnetic resonance angiography, and showed a mean detection accuracy of 95%. In addition, besides providing the MAP, the method can rank the labelings. The proposed method naturally handles anatomical structural variability and is demonstrated to be suitable for labeling arterial segments of the CoW.

Index Terms—Anatomical labeling, vascular analysis, attributed relational graph, maximum a posteriori, classification.

I. INTRODUCTION

The Circle of Willis (CoW) is a ring of cerebral arteries, located at the base of the brain, that connects the left and right anterior circulation with each other and with the posterior one, enabling a source of collateral flow in case of vascular occlusions [1]. It is also known to be a common site of pathologies, in particular of cerebral aneurysms (pathological dilations of blood vessels) [2] whose rupture can result in a subarachnoid hemorrhagic stroke, which is fatal in up to half of all the cases [3].

Many variants of CoW configuration exist, in which certain arteries are hypoplastic (very thin), missing, or duplicated [4], [5]. The standard, complete and symmetric CoW is estimated to be present in only $40 - 50\%$ of the healthy population [6], [7]. These anatomical variations in the CoW affect the volume flow rates in the feeding arteries [8]. Understanding what constitutes the normal geometric variability of CoW and what are the deviations associated with cerebrovascular pathologies is hence important and is currently still not clear. Analyzing the statistical variation of the geometry of the arteries and bifurcations constituting the CoW can lead to the identification of *geometric risk factors* [9], [10] for the onset and progress of vascular pathologies, especially aneurysms [11], [12]. To be able to register and compare CoW of different subjects, their anatomical correspondence has to be established, known as *anatomical labeling*. Manual anatomical labeling is a tedious and time consuming task. Thus, automating it becomes crucial for streamlining the geometric characterization of a large number of cases.

In particular, we are interested in anatomical labeling of the main bifurcations and arteries of the CoW (Fig. 1), where 90% of all the cerebral aneurysms occur [2]. The bifurcations represent the end points of arteries. Thus, labeling the bifurcations uniquely identifies the arteries as the vessels connecting them. To the following set of eleven bifurcations we will refer to as *bifurcations of interest* (BoI) and they identify the following arteries. Internal carotid artery (ICA), which branches into anterior cerebral artery (ACA) and middle cerebral artery (MCA). MCA is of interest up to its principal bifurcation, which divides it into the M1 and M2 segments. The two anterior circulations are connected with anterior communicating artery (AcoA), which splits the ACA into A1 and A2 segments. They are connected to the posterior tree via posterior communicating arteries (PcoA). The posterior circulation is formed by the basilar artery (BA) from which left and right posterior cerebral arteries (PCA) branch, and are further split into P1 and P2 segments by PcoA.

In this work, we present a method for automated classification of blood vessel bifurcations, which we apply to the task of anatomical labeling of the CoW. The method was designed to satisfy the following main requirements: 1) handle inter-subject variability in the topology and the number of BoI present; 2) be able to identify BoI as part of higher order furcations; 3) be robust to the presence of spurious branches

Fig. 1. Anatomy of the Circle of Willis. (a) Surface rendering. (b) Schematic representation: the artery names (in red), the inflow arteries (red arrows), and the bifurcations of interest (in blue). The arteries are: internal carotid artery (ICA), basilar artery (BA), anterior cerebral artery (ACA), posterior cerebral artery (PCA), middle cerebral artery (MCA), posterior communicating artery (PcoA) and anterior communicating artery (AcoA). Bifurcation notation: '-A' denotes anterior side, '-P' posterior, '-L' left and '-R' right.

coming from small side-branches or aneurysms; and 4) learn from newly labeled examples to improve with time. This represents an extension to the complete CoW of our previous work [13], which was focused on the anatomical labeling of the anterior circulation trees only.

The rest of the paper is organized as follows. In section II, we overview the related work in anatomical labeling of tubular structures. Section III presents the workflow of the proposed methodology. Evaluation on a set of 50 magnetic resonance angiography (MRA) images is presented in sections IV & V. Finally, section VI discusses the advantages and limitations of the proposed method and concludes the paper.

II. RELATED WORK

Anatomical labeling and anatomical matching are two related but different problems. In anatomical matching, the correspondence is sought between a pair of anatomical structures. It is normally designed for intra-patient comparison, and it assumes that the structure and/or geometry is relatively stable

between the two acquisitions. Examples are the anatomies obtained from intra-patient follow-up [14]–[16], before and after treatment [17], from different modalities [16], [18] or different phases of the breathing cycle [19], [20].

Anatomical labeling is a broader problem, where emphasis is on establishing correspondences across a population. It can be seen as a matching of an unlabeled case to an *atlas*, represented by a knowledge base of population average and the geometric and structural variability. One labeling approach is to use a pair-wise matching algorithm to match the unlabeled case with one or multiple labeled examples and then transfer the labels from the corresponding points of the best match or combine the matches in a voting scheme. Such approaches were applied for human airway tree data labeling [21]–[23]. However, the reported success rates were generally lower than the atlas-based ones, described next.

Automated anatomical labeling of 3D tubular structures in general has already attracted interest in the past. Especially the labeling of airway trees [24]–[28], as its geometry is linked to a progression of a variety of respiratory diseases. The seminal work was done by Tschirren et al. [24], where the authors match branchpoints of a target tree to the labeled reference tree, representing population atlas. Atlas is built from a training set and is represented by the mean and standard deviation values of geometric and topological features. Van Ginneken et al. [25], studied the distributions of several branch characteristics in a population. Labels are then assigned in a recursive manner, where the probability of assigning a label is conditioned on those of its children and grand children. Mori et al. in a series of works [26]–[28] developed a knowledge-based framework. For each branch of the target tree, classifier provides the likelihood of having a certain label and the combination of branch labels yielding the maximum total likelihood is chosen. However, the above methods use rigid topological constraints and does not seem to be robust to large anatomical variations in the topology.

In general, airway trees are characterized by many similar bifurcations connected by short straight branches and anatomical name changes at every bifurcation. This makes the methods designed for them difficult to apply directly to the task of labeling blood vessels which are long and tortuous and can span over many bifurcations with smaller side branches.

The early attempts of labeling vascular structures were done on coronary trees from 2D X-ray angiograms, for the purpose of their 3D reconstruction [29], [30]. These approaches match the extracted vessel skeleton graph to a 2D projection of a single 3D reference model. The variability in topology is either not considered or the appropriate reference model had to be initialized manually. Mori et al. [31] tuned their approach to a specific task of labeling abdominal arteries, where many thin arteries branch from the thick ones. Each branch is modeled with multivariate Gaussian distribution which is then used to obtain label likelihood for a given test branch. The branch-label combination that gives maximal likelihood (ML) under anatomical constraints is selected. Unfortunately, that method is anatomy specific as it divides the tree into regions and for each abdominal region different geometric arterial features are used.

To the best of our knowledge, automated anatomical labeling of the complete CoW has not been attempted in the past. The closest works related to matching or labeling cerebral arteries, besides our previous effort [13], are the ones of Tang and Chung [32], and Uchiyama et al. [33]. In [32], the authors propose a pair-wise matching algorithm that is based on combinatorial optimization strategy to compute the approximated tree edit distance (node delete and insert costs) between two anterior circulation trees obtained with 3D rotational angiography (3DRA). Their results are verified only qualitatively. In [33], the authors first rigidly register a target MRA image to the labeled reference image. Then the target arterial regions were classified into eight classes by assigning the closest label from the reference image.

Table I summarizes the results of the above methods where typical evaluation used was leave-one-out cross-validation. All of the methods were designed to label structures which have a topology of a tree. In this work, we attempt to solve a novel anatomical labeling problem where arteries form a graph structure with multiple roots and a cycle, which is a special property of the CoW. Furthermore, the proposed method is specially adapted to handle a large anatomical variability present in the topology of the CoW, and is able to compare labelings containing a highly different set of detected BoI.

III. METHODOLOGY

A. Preprocessing: from Angiographic Image to Vascular Model

In a preprocessing step for labeling, a vascular model needs to be extracted from an angiographic image. As the attributes of the model will be position and pose dependant, all images were first registered using mutual information measure and similarity transform, to the one chosen as the reference (first image in the dataset). In addition, a region of interest (ROI) around the CoW was defined on the reference image and all the registered images were cropped for the purpose of processing speed-up. The ROI is visible in Fig. 2, and was chosen with a large margin around BoI positions.

Arteries have near-circular cross-section and can effectively be modeled with their centerline and a local radius at each point [34]. Segmentation and skeletonization of the vasculature can be done with a variety of methods, as reviewed in [35], [36]. We used the following interactive inverse-skeletonization approach, where the vascular skeleton is extracted first, and the lumen second.

We first manually position seed points in all the blood vessels visible in the ROI. The centerlines are then extracted from the seeds by tracing the local intensity ridges using the method of Aylward and Bullitt [37], available within the open-source TubeTK toolkit [38]. This results in a set of centerlines, but with many being disconnected as the tracing can fail close to bifurcations. In order to connect the centerlines, from each centerline end-point we start a fast marching with underlying image intensity as a speed function, until another centerline object is reached. We then backtrack using local gradient direction to obtain the minimal cost path that connects the two centerlines [39]. We finally check that all the centerlines are

(a)

(b)
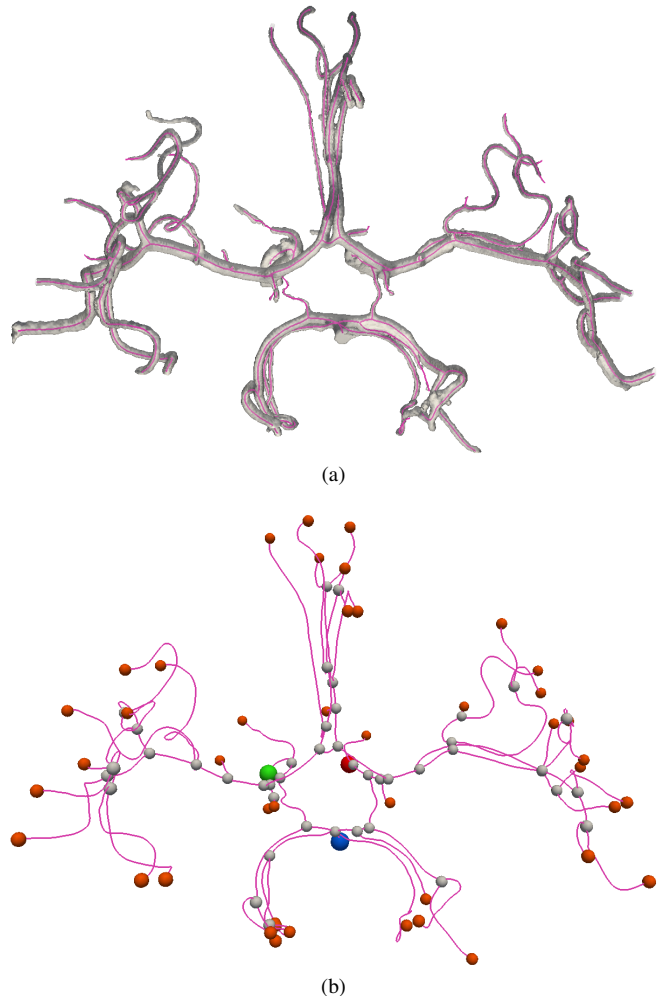
Fig. 2. Cropped region of the Circle of Willis, viewed from the top. (a) Skeleton and the lumen segmentation. (b) Skeleton represented as a graph with edges and vertices (bifurcations in gray, loose ends in orange) with the three roots: left-anterior (green), right-anterior (red), posterior (blue). (This figure is best viewed in color)

well connected and perform manual corrections if necessary. Such an approach enables us to efficiently obtain a topologically correct skeleton of the vasculature present in the image ROI.

To obtain the blood vessel radii, from the skeleton we start automated lumen segmentation using the level set based on geodesic active regions [40], [41]. Potential problem of two nearby blood vessels merging into one, especially pronounced around the parallel course of the two ACA, is avoided by using topology preserving evolution [42]. As in the level set method the segmented surface (lumen) is implicitly represented with a distance map, at the end of the evolution (Fig. 2(a)), the distance value at every skeleton point corresponds to the radius of the maximal inscribed sphere.

The extracted skeleton is modeled as a graph, where edges correspond to the individual blood vessels, while the vertices to the bifurcations and the loose vessel ends (vertices of degree one) (Fig. 2(b)). The edges describe vessels with a sequence of points (x_i, y_i, z_i, r_i), where x_i, y_i, z_i are the coronal, sagittal and axial coordinates of the centerline, respectively, and r_i is the radius.

TABLE I
OVERVIEW OF THE STATE OF THE ART METHODS IN ANATOMICAL LABELING OF 3D TUBULAR STRUCTURES.

Reference	Anatomy	Modality	# cases	# anat. labels	Accuracy rate
Tschirren et al. (2005) [24]	Airways	CT	17	32	97%
Bulow et al. (2006) [21]	Airways	CT	6	34	40-69%
van Ginneken et al. (2008) [25]	Airways	CT	36	32	90%
Mori et al. (2009) [28]	Airways	CT	90	≈ 30	86.9%
Mori et al. (2010) [31]	Abdominal arteries	CTA	89	11	84.2-88.8%
Feragen et al. (2012) [22]	Airways	CT	20	20	80.5%

The CoW can be viewed as three separate rooted trees: anterior left and right, and the posterior one; mutually connected by communicating arteries (Fig. 1(b)). The three root vertices (Fig. 2(b)), which correspond to the points where the blood flow enters the imaged field of view, are identified as the vertices (of degree one) on the lowest axial plane. Ordering them by the sagittal component, the posterior root of BA is positioned in between the left and right anterior roots of ICAs.

B. Labeling as Maximum A Posteriori Probability

The task of anatomical labeling is posed as identifying the BoI (defined in section I) on the extracted vascular model, formally considered as rooted Attributed Relational Graph (rARG).

Definition *Rooted Attributed Relational Graph* is a quadruple $\hat{G} = (V, E, A, R)$, where $G = (V, E)$ is an undirected graph with the vertex set V and the edge set E, R is the set of root vertices, and A is the set of unary vertex attributes $A : V \to F$, with F being the space of vertex features.

The labeling, in the form of a classification of bifurcations, is based on the availability of a knowledge base (KB) which consists of several elements. First, it contains a set of predefined reference graphs $\{G^r\}$. Second, from a representative sample of prelabeled graphs as a training set, it extracts the set of sample's vertex attributes $\{A^r\}$ together with the sample's set of joint BoI configurations appearing $\{V^r\}$ for each structure type. The target rARG $\hat{G}^t$ corresponds to the extracted vasculature, having its bifurcations as vertices $V^t = \{v_j^t : 1 \leq j \leq N\}$, vessels as edges E^t, root vertices as R^t, and the bifurcation attributes as $A^t = \{a_j^t\}$.

Then, on the target graph we define a labeling process as a mapping $\mathcal{L} : V^t \to V^r \cup \{\emptyset\}$, where by the null label $\emptyset$ we denote a bifurcation which is *not of interest*, and is not part of a reference G^r (Fig. 3). Mapping to the $\emptyset$ can be many-to-one, while the mapping $\mathcal{L}$ restricted to the codomain V^r is injective. Due to anatomical variability in topology, $\mathcal{L}$ is not always a surjection and the actual topology (set of BoI) detected, will be denoted with $V_{\mathcal{L}}^r = \mathcal{L}(V^t) \cap V^r$.

Our goal is to estimate the probability $P(\mathcal{L}|\hat{G}^t, KB)$ of $\mathcal{L}$ being correct. There is only one correct labeling and $\sum_{\mathcal{L}} P(\mathcal{L}|\hat{G}^t, KB) = 1$. We are then interested in finding the mode of this posterior distribution. Thus, the problem is formulated as finding a labeling $\mathcal{L}^*$ with the maximum
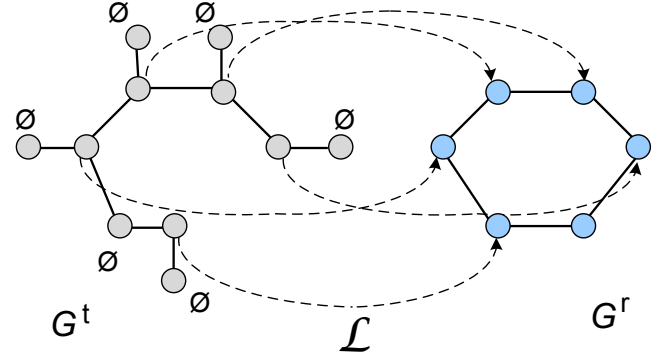
Fig. 3. Example of a labeling $\mathcal{L}$ (dotted arrows) of a target graph G^t based on a reference graph G^r with the bifurcations of interest. Vertices of both graphs can be left unmatched (denoted by $\emptyset$ on target graph).

a posteriori (MAP) probability

$$\mathcal{L}^* = \arg\max_{\mathcal{L}} P(\mathcal{L}|\hat{G}^t, KB), \tag{1}$$

where by the Bayes theorem

$$P(\mathcal{L}|G^t, A^t, R^t, KB) \propto p(A^t|\mathcal{L}, G^t, R^t, KB)P(\mathcal{L}|G^t, R^t, KB). \tag{2}$$

In such MAP estimate, the *prior* term $P(\mathcal{L}|G^t, R^t, KB)$ presents our knowledge-based expectations about the topology of the labeled target graph, where connectivities are considered but local bifurcation attributes are ignored. This prior regularizes the *likelihood* estimate $p(A^t|\mathcal{L}, G^t, R^t, KB)$, which will be considered to depend only on the local attributes. The dependence on KB will be further omitted for brevity as it is always given.

C. Likelihood Term

To estimate the likelihood term, we assume that the distribution of attributes A^t only depends locally on the bifurcation label and is independent of their connectivity E^t. Furthermore the attributes are assumed to be statistically independent between bifurcations. Thus, the likelihood term can be written and factorized as

$$p(A^t|\mathcal{L}, G^t, R^t) = p(A^t|\mathcal{L}, V^t) = \prod_{i=1}^{N} p(a_i^t|\mathcal{L}(v_i^t)). \tag{3}$$

The individual bifurcation is modeled by its origin spatial position ($\mathbf{x}$) and with its three unit vectors ($\mathbf{n}_0$, $\mathbf{n}_1$ and $\mathbf{n}_2$) pointing away from its center, in the direction the vessels

branch off (Fig. 4(a)). Such model is estimated following the objective bifurcation characterization of Antiga et al. [43]–[45]. Furthermore, each vector has a radius associated (r), obtained as the median cross-section radius of the branching vessel. Thus, each bifurcation is defined as a 7-tuple

$$a = (\mathbf{x}, \mathbf{n}_0, r_0, \mathbf{n}_1, r_1, \mathbf{n}_2, r_2) \in$$
$$\mathcal{M} = \mathbb{R}^3 \times S^2 \times \mathbb{R}^+ \times S^2 \times \mathbb{R}^+ \times S^2 \times \mathbb{R}^+. \quad (4)$$

The space $\mathcal{M}$ is a manifold endowed with the natural internal operations in each of its factors (vector addition in R^3, rotations in S^2 and multiplication in R^+), which makes it a Riemannian symmetric space.

The estimate $p(a_i^{\text{t}}|\mathcal{L}(v_i^{\text{t}}))$, i.e. the likelihood that a bifurcation with the label $\mathcal{L}(v_i^{\text{t}})$ has the unary attribute a_i^{t}, had been computed using nonlinear statistics on the manifold $\mathcal{M}$ as done similarly by Fletcher et al. [46]. To linearise the operations on the manifold Riemannian log and exponential maps are used, which map the elements of $\mathcal{M}$ to its tangent space $T_p\mathcal{M}$ at a base point $p \in \mathcal{M}$. The maps of $\mathcal{M}$ are the direct product maps of each components. For $\mathbb{R}^3$ this is the identity map. For $\mathbb{R}^+$, these are the standard logarithm and exponential functions on real variables, while for S^2 this is the spherical log and exponential map (defined in [46]). The Riemannian log map to the tangent space for the whole feature space is defined as

$$\text{Log}_p(a) = (\mathbf{x}, \text{Log}_{p_0}(\mathbf{n_0}), \log(r_0), \text{Log}_{p_1}(\mathbf{n_1}), \log(r_1),$$
$$\text{Log}_{p_2}(\mathbf{n_2}), \log(r_2)). \quad (5)$$

This tangent space is a linear space R^{12}, which will be considered Euclidean. We will denote the tangent vectors as $\mathbf{u} = (\mathbf{x}, \mathbf{v}_0, \rho_0, \mathbf{v}_1, \rho_1, \mathbf{v}_2, \rho_2)$, where $\mathbf{x} \in \mathbb{R}^3$ is the positional tangent component, $\rho \in \mathbb{R}$ is the radius tangent component ($\rho = \log(r)$), and $\mathbf{v} \in \mathbb{R}^2$ is the spherical tangent component. The Riemannian exponential map is analogously

$$\text{Exp}_p(\mathbf{u}) = (\mathbf{x}, \text{Exp}_{p_0}(\mathbf{v_0}), \exp(\rho_0), \text{Exp}_{p_1}(\mathbf{v_1}), \exp(\rho_1),$$
$$\text{Exp}_{p_2}(\mathbf{v_2}), \exp(\rho_2)). \quad (6)$$

To model the inter-subject variability of bifurcation features in a population, second order statistics are computed from the vectors $\mathbf{u_i} = \text{Log}_\mu(a_i), \mathbf{u} \in T_\mu\mathcal{M}$, in the tangent space of the intrinsic mean μ. Intrinsic (Fréchet) mean μ on a manifold is defined as

$$\mu = \arg\min_{p \in \mathcal{M}} \sum_{i=1}^{N} d(p, a_i)^2, \quad (7)$$

which can be found using gradient descent. The norm of the tangent vector $\mathbf{u} \in T_p\mathcal{M}$ is defined as

$$\|\mathbf{u}\| = (\|\mathbf{x}\|^2 + \rho_0^2 + \|\mathbf{v_0}\|^2 + \rho_1^2 + \|\mathbf{v_1}\|^2 + \rho_2^2 + \|\mathbf{v_2}\|^2)^{\frac{1}{2}}. \quad (8)$$

Then the geodesic distance between two bifurcation feature vectors $a_1, a_2 \in \mathcal{M}$ is given by

$$d(a_1, a_2) = \|\text{Log}_{a_1}(a_2)\|. \quad (9)$$

Data is assumed to be localized around the mean and is verified that the spherical tangent components $\mathbf{v_0}, \mathbf{v_1}, \mathbf{v_2}$ are lying within the distance of $\pi/2$ from the mean. Equivalently, it
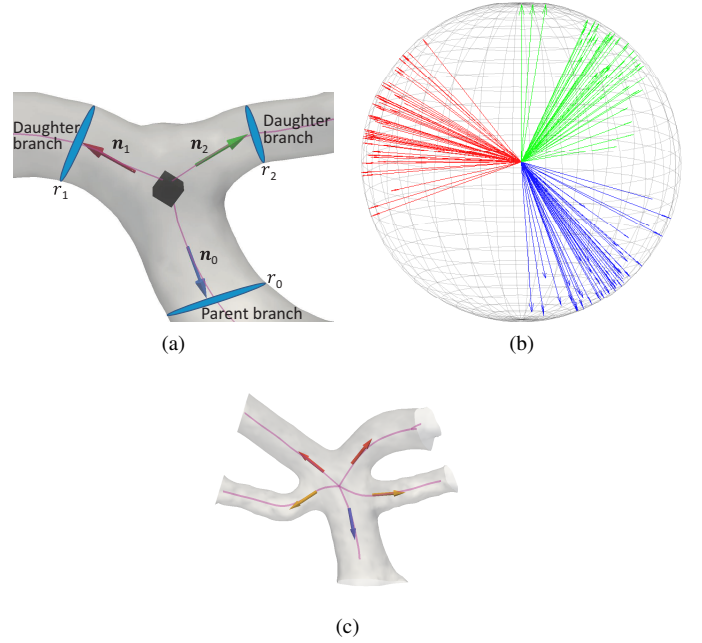
Fig. 4. Unary attributes: Bifurcation characterization (a) and distribution of bifurcation vectors in a population (b), on the example of terminal ICA bifurcation. (c) Example of BA bifurcation (parent in blue and daughters in red) forming part of a quadfurcation. (This figure is best viewed in color)

is visually confirmed that individual bifurcation vectors of the population are distributed within one hemisphere (Fig. 4(b)).

The likelihood is then estimated from multivariate normal distribution as

$$p(a_i^{\text{t}}|\mathcal{L}(v_i^{\text{t}})) = \frac{1}{\sqrt{(2\pi)^k |\mathbf{S}|}} \exp(-\frac{1}{2}D^2), \quad (10)$$

where k is the dimension of the space, D is the Mahalanobis distance $D = \mathbf{u}^T\mathbf{S}^{-1}\mathbf{u}$, and $\mathbf{S}$ is the covariance matrix of the label $\mathcal{L}(v_i^{\text{t}})$, estimated from the sample as $\mathbf{S} = \frac{1}{N-1}\sum_{i=1}^{N} \mathbf{u_i}\mathbf{u_i}^T$. The covariance matrix $\mathbf{S}$ is specific to each label, as different reference bifurcations will have different variabilities. The proposed representation is especially suitable when BoI appears as part of higher order furcations (Fig. 4(c)), which is handled by selecting the combination of three branches that minimize the Mahalanobis distance to the corresponding mean feature element.

Ideally, given a large amount of training data, the above Eq. 10 would be computed for the full $k = 12$ dimensional space. However, for a more limited data, due to the *curse of the dimensionality* problem, such a large number of parameters affects the generalization capability of the Bayes estimator. Thus, we split the likelihood as a product of separate likelihood estimates for: 3D space of positions, $3 \times 2D$ tangent space of bifurcation vectors and 3D tangent space of radii.

Finally, it is necessary to define the likelihood for assigning a null label ø to a vertex, i.e. $p(a_i^{\text{t}}|\text{ø})$. In the absence of any other information, we assume that the bifurcations corresponding to ø are uniformly distributed on the reachable finite region of the manifold $\mathcal{M}$. For positional $\mathbb{R}^3$, the uniform distribution in a fixed cuboid region of interest (ROI), defined by expected BoI position range, with volume V_{ROI} has a constant value of

$1/V_{\text{ROI}}$. The space $\mathbb{R}^+$ is limited to the expected range of radii values, producing $\frac{1}{\log r_{\max} - \log r_{\min}}$. Uniform distribution on the whole unit sphere S^2 has a value of $\frac{1}{4\pi}$. Thus, we obtain:

$$p(a_i^{\text{t}}|\emptyset) = \frac{1}{V_{\text{ROI}}} \left(\frac{1}{4\pi} \right)^3 \left(\frac{1}{\log r_{\max} - \log r_{\min}} \right)^3, \quad (11)$$

where the expected ranges are obtained from the training set.

D. Prior Term

Vasculature of CoW exhibits big variability in its topology, and for many subjects not all BoI are present. Furthermore, some BoI are more probable to be missing than others and absence of one bifurcation can imply that others further downstream cannot be present either. In addition, bifurcations can only appear in certain ordering, starting from the roots. Thus, the use of the prior term has a double role. First, it models the probability distribution of topologies $\{V_{\mathcal{L}_j}^{\text{r}}\}$, i.e. the probability that the detected BoI combination appears. Second it assures that the labeling is *compatible* with the reference graph i.e. the labels assigned to the target graph follow the ordering they have on the reference graph. How is the ordering defined on a graph with a cycle is explained in subsection III-F.

Formally, prior term restricts the set L^{t} of all possible labelings of the target only to the *compatible* ones $\mathcal{L} \in L_{\text{c}}^{\text{t}} \equiv \{\mathcal{L}_1, \ldots, \mathcal{L}_Q\}$, each with its corresponding set of involved BoI $\mathbf{V}_c^{\text{r}} \equiv \{V_{\mathcal{L}_1}^{\text{r}}, \ldots, V_{\mathcal{L}_Q}^{\text{r}}\}$. Then we can write:

$$P(\mathcal{L}|G^{\text{t}}, R^{\text{t}}) = \begin{cases} 0 & \text{if } \mathcal{L} \notin L_{\text{c}}^{\text{t}} \\ P(i|V^{\text{t}}, E^{\text{t}}, R^{\text{t}}, L_{\text{c}}^{\text{t}}) & \text{if } \mathcal{L} \in L_{\text{c}}^{\text{t}}; \mathcal{L} = L_{\text{c}}^{\text{t}}(i) \end{cases} \quad (12)$$

where $P(i)$ denotes the probability that the correct labeling is at the ith indexed position in the set of *compatible* labelings.

The probability distribution of the non-zero prior $P(i|V^{\text{t}}, E^{\text{t}}, R^{\text{t}}, L_{\text{c}}^{\text{t}}, \mathbf{V}_c^{\text{r}})$, can then be obtained under certain assumptions. It is first assumed that the probability of a particular labeling from the set L_{c}^{t} will be independent of the particular E^{t} and R^{t}:

$$P(i|V^{\text{t}}, E^{\text{t}}, R^{\text{t}}, L_{\text{c}}^{\text{t}}, \mathbf{V}_c^{\text{r}}) = P(i|V^{\text{t}}, L_{\text{c}}^{\text{t}}, \mathbf{V}_c^{\text{r}}). \quad (13)$$

Thus, the locations of $\emptyset$ do not affect the prior probability. We further assume that the prior probability only depends on the detected topology $V_{\mathcal{L}}^{\text{r}}$ and is independent of the particular vertices of V^{t} that map to the $V_{\mathcal{L}}^{\text{r}}$, as long as $\mathcal{L} \in L_{\text{c}}^{\text{t}}$. Thus,

$$P(i|V^{\text{t}}, L_{\text{c}}^{\text{t}}, \mathbf{V}_c^{\text{r}}) = P(i|\mathbf{V}_c^{\text{r}}) \propto P(\mathbf{V}_c^{\text{r}}|i)P(i) \propto P(\mathbf{V}_c^{\text{r}}|i), \quad (14)$$

where we have considered that $P(i)$ is constant, i.e. the order of the labelings in the set L_{c}^{t} is arbitrary. Lastly, given that the correct labeling $\mathcal{L}$ is in the position i ($\mathcal{L} = \mathcal{L}_i$) we assume that the prior only depend on $V_{\mathcal{L}_i}^{\text{r}}$ and that the presence of any other set of compatible topologies in the set L_{c}^{t} is equally probable and independent of $\mathcal{L}_i$:

$$P(\mathbf{V}_c^{\text{r}}|i) \propto P(V_{\mathcal{L}_i}^{\text{r}}|i) = P(V_{\mathcal{L}}^{\text{r}}) \quad (15)$$

Finally, the prior term can then be summarized as

$$P(\mathcal{L}|G^{\text{t}}, R^{\text{t}}) = \begin{cases} 0 & \text{if } \mathcal{L} \notin L_{\text{c}}^{\text{t}} \\ P(V_{\mathcal{L}}^{\text{r}}) & \text{if } \mathcal{L} \in L_{\text{c}}^{\text{t}} \end{cases} \quad (16)$$

E. Reference Graphs

The anatomical variability of CoW is reflected in the presence/absence of the three communicating paths between the roots. Based on that, we define eight different high level structure types $\{\text{ST1}, \ldots, \text{ST8}\}$, and for every structure type we added a reference graph to KB (Fig. 5). All the reference graphs have all the BoI present. This is because the communicating paths do not necessarily have to be cut at the communicating arteries, as ACA-A1 or PCA-P1 segments could also be missing and the communicating arteries AcoA and PcoA would connect directly to ACA-A2 and PCA-P2 segments, respectively (example in Fig 6). Thus, we cannot deduce beforehand which of the BoI are missing and such lower scale ambiguities and the actual topology have to be resolved later by the labeling method.

F. Vertex Ordering on a Graph with a Cycle and Multiple Roots

To establish an ordering of vertices on a graph with a cycle, to each root $r_k \in R, k \in \{1, 2, 3\}$ we associate a directed graph (digraph) $G_k = (V, S(r_k))$, where $S(r_k)$ is a set of ordered vertex pairs $S(r_k) \subset V \times V$. In the case of the complete CoW, to each root vertex r_k we associate a corresponding *joining vertex* o_k, where the root connects to the cycle (denoted with squares in Fig. 5(a)). Then, $(v_i, v_j) \in S(r_k)$ iff there exists a simple path from r_k to v_j, passing through v_i, but not through any of its non-corresponding *joining vertices* $o_{k'}$ for $k' \neq k$. Thus, each root r_k induces a partial order on vertices through digraph reachability relationship specified by $S(r_k)$. We can then complement every rARG with this derived structure, to obtain $\bar{G} = (V, E, A, R, \{S(r_k)\})$.

This definition is applicable to target as well as to reference graphs. The root-specific digraphs (denoted with arrows in Fig. 5), are obtained by performing from each root a breadth-first order vertex traversal, preventing the transversal beyond its non-corresponding joining vertices. The labeling of the target graph will then be considered *compatible* (Eq. 12) with the reference graph if labels on the target digraphs G_k^{t} preserve the partial order of the reference digraphs G_k^{r}. More formally, if for all pairs of the assigned labels which are in $S^{\text{r}}(r_k)$ their corresponding pair of target vertices is in $S^{\text{t}}(r_k)$, for all roots:

$$(V_{\mathcal{L}}^{\text{r}} \times V_{\mathcal{L}}^{\text{r}}) \cap S^{\text{r}}(r_k) \subseteq \mathcal{L}(S^{\text{t}}(r_k)), \quad \forall r_k. \quad (17)$$

G. Reference Graph Selection

The labeling method requires that the target and the reference graph induce compatible partial orders from their roots. Thus, we need to identify the target structure type and select the reference graph of the same type. For that, we observe the mutual reachability of the three roots. If all the roots are mutually reachable, to additionally detect whether the CoW is complete we search for the cyclic path in the graph.

From the above observations we can then identify directly 5 out of 8 structure types (Table II), with ambiguity remaining between ST2, ST3, and ST4 (all roots are mutually reachable and there is no cycle). In such ambiguous cases, we perform
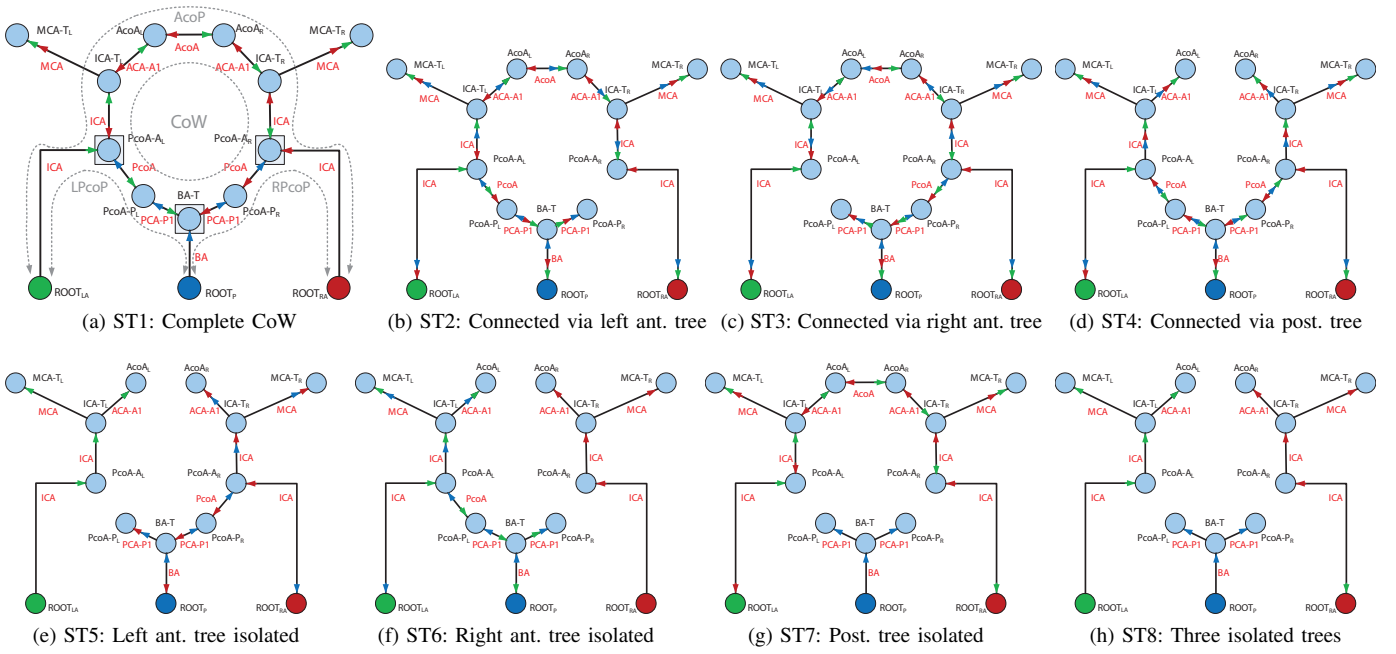
Fig. 5. The eight reference graphs, where bifurcation and artery names correspond to the Fig. 1. Digraph induced by each root is shown with arrows in corresponding color: left-anterior (green), right-anterior (red) and posterior (blue). In addition, (a) shows: The communicating paths (gray) between the roots of the trees: anterior communicating path (AcoP), left posterior communicating path (LPcoP) and right posterior communicating path (RPcoP). The *joining vertices* (squares), where the three roots connect to the CoW cycle. (This figure is best viewed in color)
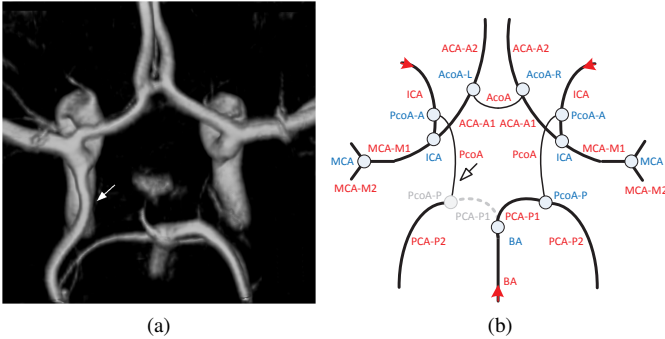
Fig. 6. (a) Volume rendering of a subject with P1 segment missing, where the left PcoA (denoted with arrow) takes the role of the left PCA. (b) Schematic representation (arrow at the same position as in (a)), where missing parts are grayed out (compare with Fig. 1). Thus, PcoA-A bifurcation is present but not PcoA-P.

TABLE II
GRAPH STRUCTURE TYPES AND THEIR PROPERTIES. THE PRESENCE OF COMMUNICATING PATHS BETWEEN THE TREES (ABBREVIATIONS FOLLOW FIG. 5); THE MUTUAL REACHABILITY OF THE THREE ROOTS: LEFT-RIGHT (LR), LEFT-POSTERIOR (LP), AND RIGHT-POSTERIOR (RP); THE PRESENCE OF THE COW CYCLE.

Type ID	Communicating Paths			Root Reachability			Cycle
	AcoP	LPcoP	RPcoP	LR	LP	RP	
ST1	1	1	1	1	1	1	1
ST2	1	1	0	1	1	1	0
ST3	1	0	1	1	1	1	0
ST4	0	1	1	1	1	1	0
ST5	0	0	1	0	0	1	0
ST6	0	1	0	0	1	0	0
ST7	1	0	0	1	0	0	0
ST8	0	0	0	0	0	0	0

three separate labelings with each of the three possibly corresponding reference graphs, having the same prior $P(G^r)$. We then combine all the resulting labelings, expecting that those based on incompatible reference graphs will produce very low posterior probabilities.

Finally, the selection of the reference graph affects the prior term (subsection III-D) as the set of compatible labelings are reference-specific. Thus, $P(V_{\mathcal{L}}^r)$ becomes $P(V_{\mathcal{L}}^r|G^r)$ (in Eq. 15 & 16). In addition, since each of the 8 reference types is characterized by the presence status of each of the 3 communicating paths, we use it to adapt the prior probability of detecting BoI on them. Considering the probability of presence of BoI belonging to different paths to be independent,

we obtain:

$$
\begin{aligned}
P(V_{\mathcal{L}}^r|G^r) &= P(V_{\mathcal{L}}^r|\text{AcoP}, \text{LPcoP}, \text{RPcoP}) = \\
&= P(\text{ICA}_L, \text{AcoA}_L, \text{AcoA}_R, \text{ICA}_R|\text{AcoP}) \cdot \\
&\quad \cdot P(\text{PcoA-A}_L, \text{PcoA-P}_L|\text{LPcoP}) \cdot \\
&\quad \cdot P(\text{PcoA-A}_R, \text{PcoA-P}_R|\text{RPcoP}) \cdot \\
&\quad \cdot P(\text{MCA}_L)P(\text{MCA}_R)P(\text{BA}),
\end{aligned}
\tag{18}
$$

where the BoI and path names (from Fig. 5(a)) denote their presence status: present or absent.

H. Optimization

MAP estimation, in general, is very computationally expensive. Exhaustive testing for all possible labelings $\mathcal{L} \in L^t$ is not feasible. However, many vertex-label pairings can be automatically discarded based on either zero prior probability or low

likelihood. In fact, the *prior* probability $P(\mathcal{L}|G^t, R^t)$ is non-zero only for a small subset of all combinations ($\mathcal{L} \in L_c^t$) i.e. only for those which are compatible with the reference graph. To avoid labelings involving very low probable attributes, we exclude outliers based on their Mahalanobis square distance D^2. Under multivariate normal distribution assumption, it is a χ^2 distribution. We then detect the outliers at 99.999% cutoff level.

The labeling is a morphism $\mathcal{L} \subseteq V^t \times (V^r \cup \emptyset)$. A standard algorithm for mapping between two graphs is based on building their association graph and then finding *maximal cliques* of such an undirected graph [47], [48]. Association graph $G = (V^a, E^a)$ is built from G^t and G^r, where nodes are denoted with a pair of indices $V^a = \{v_{i,j}^a \equiv (v_i^t, v_j^r)\} \subset V^t \times (V^r \cup \{\emptyset\})$. The following rules are applied. Node is created only if unary attribute of v_i^t with the label of v_j^r is not considered an outlier. Edge $(v_{i,j}^a, v_{k,l}^a)$ is created for $i \neq k$ and $j \neq l$, unless $(v_j^r, v_l^r) \in S^r(r_k)$ and $(v_i^t, v_k^t) \notin S^t(r_k)$ for any r_k, ensuring ordering compatibility. Edges pairing with the $\emptyset$ are always created.

Finding maximal cliques, which in our case will always be of the size N of the target graph, in an undirected graph is in general a NP-complete problem. However, removing the nodes of the association graph detected as outliers, cuts down the computational effort to a manageable size. Here any clique finding algorithm can be used [49]. We used the algorithm and C implementation of Tomita et al. [50], in which pruning methods are employed to reduce the size of search space, and where benchmarks showed that it runs very fast in practice.

IV. EVALUATION METHODOLOGY

We evaluated the proposed methodology on a set of 50 images of healthy volunteers (25 male, 25 female, age range: 19-66, mean age: 39), acquired with time-of-flight (ToF)-MRA on a 3T unit under standardized protocols. Images were reconstructed with $448 \times 448 \times 128$ matrix, having a voxel size of $0.5 \times 0.5 \times 0.8$ mm³. The images come from the dataset used in [51], which is freely available as open data[1].

The performance of BoI classification was evaluated using leave-one-out cross-validation. Two clinicians manually labeled the BoI on each vascular model. The labels of the first clinician were considered as the ground truth, while the labels of the second were used to detect and measure any inter-observer variability. All the other bifurcations were assigned the $\emptyset$ label. For each BoI we report detection accuracy, precision, sensitivity and specificity rates. In addition, we compute *per case* rate of correctly labeling all the BoI, as well as the rate of detecting the topology only: whether the set of BoI determined to be present is correct, disregarding their position. Furthermore to evaluate how is the classification performance affected by the training set size, we additionally ran the cross-validation with six different image subset sizes (45, 40, 35, 30, 25, and 20 images). For each subset size, the cross-validation was repeated with five different random subsamples.

[1]http://hdl.handle.net/1926/594

To evaluate the contribution of different elements of the method, we repeated the performance analysis for different method variants. The first variant (AT) is based just on the unary attributes without taking the graph and its node connectivity, nor prior term into account. Such variant can be seen as an adaptation of the labeling presented in [33], [52]. The second variant (AT+G) is using the unary attributes and the graph preserving ordering, but without the prior term. This can be considered as an adaptation of the approaches of [24], [31]. The last two variants correspond to the proposed method with two different prior terms. One prior term (AT+G+AP) contains overall population appearance probabilities independent of the reference graph used, while the other (AT+G+AP+R) further adapts them based on the structure type of the chosen reference graph (Eq. 18). To evaluate whether the learned prior was data specific, we additionally repeated the AT+G+AP and AT+G+AP+R labelings using the values of anatomical variants prevalence reported in [7], where the authors visually inspected 150 ToF-MRA images of healthy volunteers.

The method ranks the candidate labelings by their estimated posterior probabilities, and always selects the most probable one (the highest ranked one). However, in the case that selected labeling is visually observed to be incorrect, this enables a user to quickly select the next most probable candidate in the ranked list. To evaluate the ranking success, for the erroneously labeled cases we search how distant in the ranked list is the correct labeling.

Finally, to test the robustness of the method to the presence of pathologies, we further included ToF-MRA images from 6 patients (Hospital Clinic, Barcelona, Spain) bearing one or more cerebral aneurysms. Distribution of the cerebral aneurysms was the following: MCA (3 on the bifurcation and 1 mid-branch), ICA-PcoA bifurcation (2), BA (1), ICA terminal bifurcation (1).

V. RESULTS

Examples of anatomical labeling results are shown in Fig. 7, where the surface of each corresponding vessel segment is color labeled. The classification performance is shown in Table III. It can be observed that the BoI detection rates are high, but unfortunately the errors are evenly spread across cases so only 58% of the cases are labeled entirely correctly. The effect of training set size on labeling all BoI correctly, and topology detection is shown in Fig. 8. The performance seems to stabilize when 40 or more images were used for training, but drops noticeably when less than 35 subjects were used.

Most of the detection errors are in locating the MCA terminal bifurcation (Fig. 7(e) & (f)). Excluding MCA, 84% of cases would be correctly labeled. The difficulty in locating this bifurcation is not unexpected as the MCA has the most complex branching pattern of any of the major cerebral arteries [53], [54].It was the only BoI where inter-observer variability of labeling existed, with the two clinicians having agreement of 89%. Furthermore, MCA is always present ($P(\text{MCA}) = 1.00$ in Eq. 18) and is outside the cycle forming the CoW with no other BoI further downstream, hence the connectivity and prior term are not contributing to its localization.
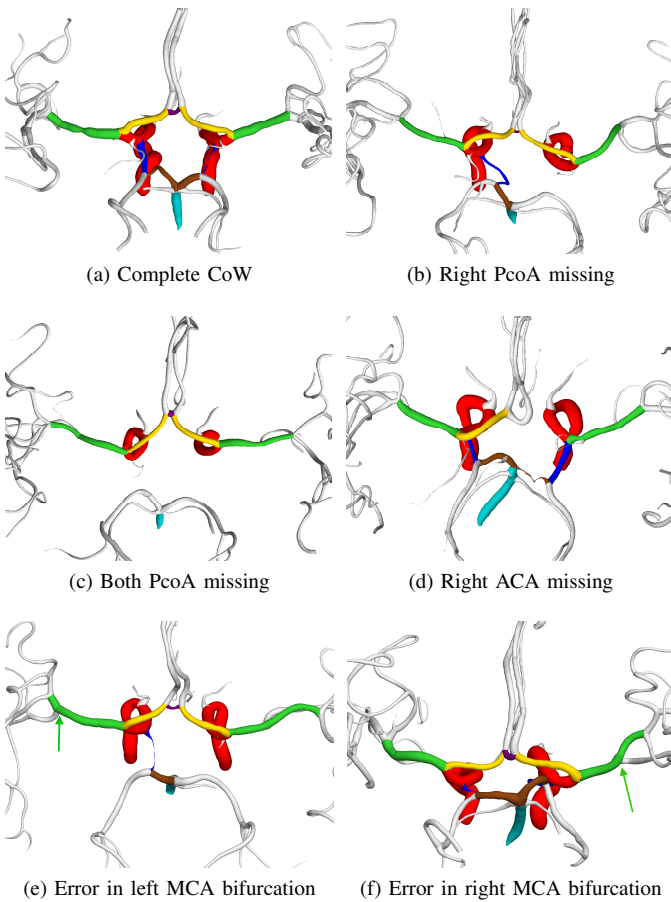
Fig. 7.   Anatomically labeled Circle of Willis. Denoted vessels: ICA (red), BA (turquoise), ACA (yellow), PCA (brown), PcoA (blue), AcoA (purple), MCA (green). Correct labeling is shown in (a-d). Examples of incorrect MCA labeling are shown in (e,f), where the arrow denotes the true terminal bifurcation. (This figure is best viewed in color)

In general, the result shows that the method favors sensitivity over specificity, i.e. it finds false BoI rather than miss one. This can be attributed to the conservative size of the finite reachable region of the feature space used in estimating the ø-label likelihood (Eq. 11). The region was guaranteed to include any bifurcation, with the risk of being too large. Of the false positives, most appeared due to mistaking a small side branch for a communicating artery (PcoA or AcoA), when the latter was actually missing. In particular, anterior choroidal artery, which is located just next to PcoA and branches in the same direction, can be mistaken for a PcoA branching from the anterior side and not connecting with the posterior root.

The performance of different method variants is shown in Table IV. Gradually adding the regularization terms improved the performance across the rates. In particular, adding the prior term clearly improved the specificity and topology detection. With it, some bifurcations with side branches are prevented from assigning a BoI label as otherwise they would form configurations which are uncommon in a population. In particular the reference graph based prior was shown effective and improved specificity and topology by $\sim 10\%$. With just AP prior, the false positive communicating arteries appeared. By using AP+R prior, these errors are avoided as they would be

TABLE III
PERFORMANCE ANALYSIS OF THE PROPOSED METHOD. N/A DENOTES "NOT AVAILABLE" (0/0). THE MEAN VALUES ARE WEIGHTED ACROSS BoI.

Bifurcation of Interest	Detection			
	Accuracy	Precision	Sensitivity	Specificity
ICA_L	1.00	1.00	1.00	N/A
ICA_R	0.98	1.00	0.98	1.00
$PcoA_{FL}$	0.98	1.00	0.97	1.00
$PcoA_{FR}$	0.98	0.97	1.00	0.93
$AcoA_L$	0.96	0.95	1.00	0.88
$AcoA_R$	1.00	1.00	1.00	1.00
$PcoA_{BL}$	0.96	0.95	1.00	0.87
$PcoA_{BR}$	1.00	1.00	1.00	1.00
BA	0.96	0.96	1.00	N/A
MCA_L	0.80	0.80	1.00	N/A
MCA_R	0.84	0.84	1.00	N/A
Mean	0.95	0.95	0.99	0.95
Per case	Labeling all correct: 58%, Topology correct: 88%			
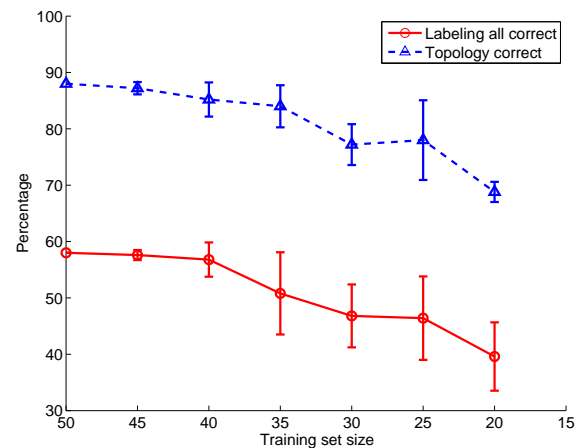
Fig. 8.   Influence of the training set size on the labeling performance.

TABLE IV
COMPARISON OF MEAN PERFORMANCE VALUES BETWEEN THE METHOD VARIANTS.

Method	Detection mean rates				Topology
	Acc.	Prec.	Sens.	Spec.	
AT $\sim$ [33], [52]	0.91	0.91	0.98	0.76	64%
AT+G$\sim$ [24], [31]	0.92	0.93	0.98	0.81	62%
AT+G+AP	0.93	0.93	0.98	0.85	76%
AT+G+AP+R	0.95	0.95	0.99	0.95	88%

contradictory with the property of having disconnected roots.

Evaluation of ranking success is shown in Fig. 9. Using the prior term clearly helps to position correct labelings higher in the ranking list, and for 90% of cases the correct labeling is within the first ten positions. Figure 9 also shows the results with prior term exclusively based on data from [7]. The obtained rankings were similar, which shows that the learned prior and the data used could be representative of the normal healthy population. Comparison (Table V) of the prevalence of anatomical variants learned from this data with the one reported in [7] showed similar values with no statistically significant differences ($p > 0.05$).
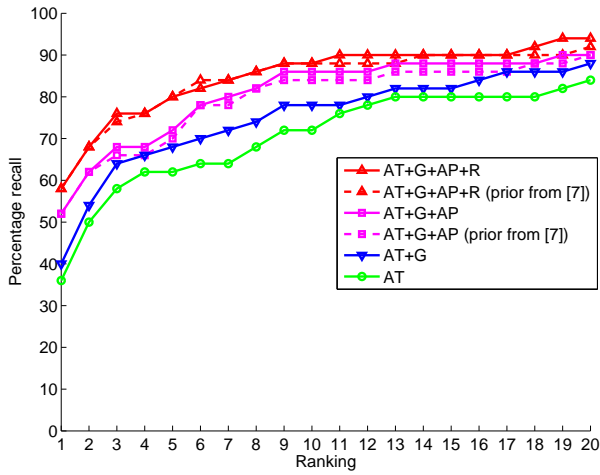
Fig. 9.   Percentage of cases with the correct labeling appearing ahead or equal the given rank, for the method variants.

TABLE V
PREVALENCE OF THE MAIN ANATOMICAL VARIANTS. COMPARISON BETWEEN THE REFERENCE STUDY [7] (150 SUBJECTS) AND THE VALUES LEARNED FROM THIS DATA (50 SUBJECTS). NUMBERS REPRESENT PERCENTAGE OF SUBJECTS WITH THE GIVEN TOPOLOGICAL PROPERTY.

	Hartkamp et al. [7]	Learned data
Complete CoW	42%	34%
Complete anterior part	74%	80%
AcoA missing	19%	16%
A1 segment missing	7%	4%
Complete posterior part	52%	48%
Both PcoA missing	11%	12%
Unilateral PcoA missing	33%	30%
P1 segment missing	4%	10%

Finally, we tested the algorithm on the 6 images containing cerebral aneurysms. For 5 out of 6 images the bifurcation and the artery containing an aneurysm was correctly labeled (Fig. 10). On the one image where the MCA bifurcation with aneurysm was erroneously labeled, the result was equally wrong when the aneurysm was manually removed. Thus, the presence of the aneurysms did not influence the labeling results. When an aneurysm appears mid-branch, for the method it is just an extra spurious branch and the bifurcation gets label ø assigned. When it appears as part of BoI, it turns a n-furcation into n+1-furcation, but the method is able to identify the correct subset of branches belonging to BoI (analogous to Fig. 4(c)).

VI. DISCUSSION

In this work we developed a method for labeling main arteries of the CoW, known to exhibit large anatomical variability. In the dataset used for evaluation, the complete CoW was present in one third of the cases (34%), hence encountering missing arteries was the norm, not the exception. The proposed labeling method is based on combining BoI attributes and their graph connectivity with the prior probability of encountering the global topology they form. From a training set of prelabeled examples, the method was able to learn bifurcation feature variability as well as variation in

(a) MCA mid-branch

(b) MCA bifurcation

(c) ICA-PcoA bifurcation and ICA mid-branch

(d) ICA bifurcation (two-dome aneurysm)
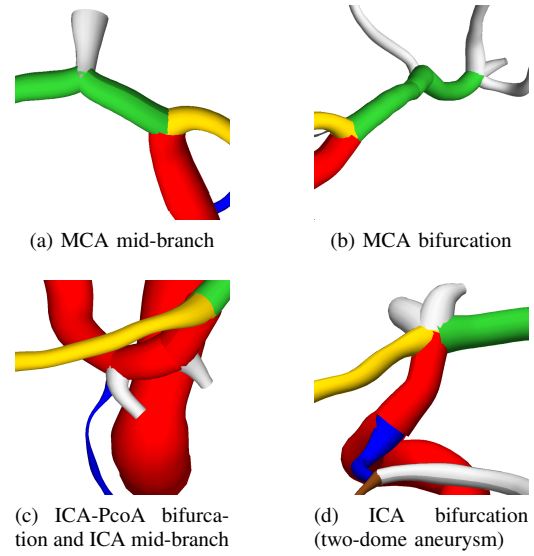
Fig. 10.   Example of anatomical labeling in the presence of aneurysms at different locations. Color scheme follows the one of Fig. 7. (This figure is best viewed in color)

topology and their probabilities of occurrence. We also tested substituting prior probabilities with the ones from [7], which showed that the method could integrate the values from other, future studies, which analyze anatomical variability of CoW of a large population, in sufficient detail.

Bifurcations are characterized as points in a Riemannian manifold, and statistics computed in tangent space, which was inspired by the work on medial representation atoms [55], [56]. Bifurcations not of interest (ø label) are then modeled as uniformly distributed on the finite region of the feature space. Being able to estimate likelihood for assigning ø is crucial for comparing labelings containing different number of BoI detected, the first design requirement. Furthermore, the chosen characterization enables identifying the BoI when being a part of higher order furcation by selecting the triplet of branches that minimize the Mahalanobis distance to the mean feature element, the second design requirement. The labeling is posed as the classification of BoI rather than arteries directly. As artery can have several side-branches or aneurysms, finding its start and end bifurcations makes the method robust to the presence and the number of such spurious branches, the third design requirement. Finally, the method also ranks the labeling candidates to easily search for the correct solution if needed, which can then be fed back to the training set and improve future performance, the fourth design requirement.

The method supports graphs that contain a cycle and have multiple roots, as long as each root is attached to the cycle at a different node, which allows to split the graph into multiple digraphs. Each digraph induces partial order on its nodes and enables finding reference topology preserving labelings. Such labelings are obtained by computing maximal cliques of the association graph, which is a standard method for graph matching [47]. Although finding maximal cliques is known to be NP-hard, it is a well studied problem and powerful heuristics exist which efficiently find good approximate so-

lutions. In our application, it was computationally feasible to find all maximal cliques, as the association graph could be substantially pruned by removing outlier pairing nodes based on local features. With the pruned association graph having ~ 70 nodes, maximal cliques were found in a few seconds, using the C implementation. However, for applications involving a larger number of BoI, more efficient optimization strategy should be employed.

A limitation of our method is that BoI merging is not supported. There is a known anatomical variability where AcoA's length reduces to a point (AcoA$_L$ and AcoA$_R$ bifurcations merge), but it is rare (1.3% prevalence in [7]) and is not taken into account in this work. In general this could be handled in a labeling post-processing step, by analyzing a bifurcation that has a high likelihood of being two neighboring BoI. Furthermore, we do not make use of any binary (edge) attributes. They might further improve the robustness of the method, but also introduce difficulty in modeling the likelihood of ø assignments, and the treatment of spurious side branches. Finally, as the segmentation was performed on ToF-MRA images, we were not able to distinguish between the case when an artery was missing due to anatomical variability and the case when it was present but not enhanced due to its small blood flow. However, from the application point of view, distinguishing between the two cases is of minor importance as the role of an artery unable to conduct large blood flow, is negligible in flow regulation of the CoW.

The topological correctness of the segmentation is assumed for the labeling method to work properly. Accurate and robust extraction of cerebral arteries remains an open problem that affects any artery and bifurcation labeling method. Thus in the pre-processing step, through manual interaction (~ 20 min per case) we assured that the extracted skeleton had the correct topology. It also enabled the labeling method to make use of the BoI ordering, and to evaluate the detection rates without the results being influenced by the segmentation success. In the case an automated segmentation is required, which does not produce topologically correct skeletons, the labeling method should discard the vertex ordering and treat all possible labelings as being compatible with the reference. This would increase the method's computation time and decrease the detection rates.

The performance comparison with the related work is difficult, as none are directly applicable to the CoW. Thus, we created variants of the proposed method which are adaptations of the concepts used elsewhere. The results showed that the proposed MAP method outperformed the ML-based one. The method has been evaluated on open data, which should facilitate future comparisons with other methods and studies.

Overall, the BoI were detected with high (95%) accuracy and precision. These rates are comparable to the ones obtained by the state of the art methods designed for other anatomies (Table I). However, it had a relatively low success rate (58%) of completely labeling the entire CoW. Errors were focused mostly around the location of MCA terminal bifurcation which is known to be hard to identify. As a comparison, other related works unfortunately avoided reporting the per case labeling success. It can be read only from the results of [24], where

it would correspond to the per case labeling success of 47% (8/18). This hints that similar, low overall performances, are expected to be present in other works, and shows the difficulty and future challenges in designing a successful labeling method. That is why we proposed to find all topologically valid labelings and rank them by their posterior probability. For erroneously labeled cases, the evaluation showed that the correct solution was most frequently ranked second.

The main contributions of the presented work are the following:

- Characterizing the bifurcations as points on a Riemannian manifold, which concisely models the bifurcations and hence increases the generalization property of the likelihood estimator.
- Modeling the features of ø-label as being uniformly distributed on the manifold, to compare between labelings involving different number of labels present.
- Introduction of a priori probabilities of label configuration appearance, to regularize the labeling's likelihood estimate.
- Method for defining partial order on graphs with a cycle and multiple roots, to make use of the BoI ordering on the CoW.

The methodology (section III), is posed general and can find application in labeling other tubular or vascular structures, apart from CoW. Structures where the underlying graph has cycles, can be observed at the level of capillary networks. In addition, in many organs, arteries can directly fuse (anastomose) with each other, forming collateral circulation, which can appear naturally or as a result of pathology remodeling.

The proposed labeling method was designed as a step toward the extensive geometric characterization of the CoW. Apart from topology and bifurcations geometry, the geometry of individual vessels can further be characterized using the technique proposed in [57]. Having such complete characterization of CoW in a population is of value in the pursuit of identifying geometric risk factors, a goal of the future work.

REFERENCES

[1] A. G. Osborn and J. M. Jacobs, *Diagnostic cerebral angiography*, 2nd ed. Lippincott Williams & Wilkins, 1999.

[2] J. L. Brisman, J. K. Song, and D. W. Newell, "Cerebral aneurysms," *N. Engl. J. Med.*, vol. 355, no. 9, pp. 928–939, Aug. 2006.

[3] J. van Gijn, R. S. Kerr, and G. J. E. Rinkel, "Subarachnoid haemorrhage," *Lancet*, vol. 369, no. 9558, pp. 306–318, Jan. 2007.

[4] M. J. Hartkamp and J. van der Grond, "Investigation of the circle of Willis using MR angiography," *Medicamundi*, vol. 44, no. 1, pp. 20–27, Mar. 2000.

[5] S. J. Dimmick and K. C. Faulder, "Normal variants of the cerebral circulation at multidetector CT angiography," *RadioGraphics*, vol. 29, no. 4, pp. 1027–43, Jan. 2009.

[6] B. J. Alpers, R. G. Berry, and R. M. Paddison, "Anatomical studies of the circle of Willis in normal brain," *AMA Arch. Neurol. Psychiatry*, vol. 81, no. 4, pp. 409–418, Apr. 1959.

[7] M. J. Krabbe-Hartkamp, J. van der Grond, F. E. de Leeuw, J. C. de Groot, A. Algra, B. Hillen, M. M. Breteler, and W. P. Mali, "Circle of Willis: morphologic variation on three-dimensional time-of-flight MR angiograms," *Radiology*, vol. 207, no. 1, pp. 103–111, Apr. 1998.

[8] J. Hendrikse, A. F. van Raamt, Y. van der Graaf, W. P. T. M. Mali, and J. van der Grond, "Distribution of cerebral blood flow in the circle of Willis," *Radiology*, vol. 235, no. 1, pp. 184–189, Apr. 2005.

[9] M. H. Friedman, O. J. Deters, F. F. Mark, C. B. Bargeron, and G. M. Hutchins, "Arterial geometry affects hemodynamics. a potential risk factor for atherosclerosis," *Atherosclerosis*, vol. 46, no. 2, pp. 225–231, Feb. 1983.

[10] M. H. Friedman, "Variability of 3D arterial geometry and dynamics, and its pathologic implications," *Biorheology*, vol. 39, no. 3-4, pp. 513–517, 2002.

[11] K. N. Kayembe, M. Sasahara, and F. Hazama, "Cerebral aneurysms and variations in the circle of Willis," *Stroke*, vol. 15, no. 5, pp. 846–850, Sep. 1984.

[12] J. R. Cebral, M. A. Castro, J. E. Burgess, R. S. Pergolizzi, M. J. Sheridan, and C. M. Putman, "Characterization of cerebral aneurysms for assessing risk of rupture by using patient-specific computational hemodynamics models," *AJNR Am. J. Neuroradiol.*, vol. 26, no. 10, pp. 2550–2559, Nov. 2005.

[13] H. Bogunovic, J. M. Pozo, R. Cardenes, and A. F. Frangi, "Anatomical labeling of the anterior circulation of the circle of Willis using maximum a posteriori classification," in *Proc. Int. Conf. Med. Imag. Comput. & Comput. Assist. Interven. (MICCAI)*, ser. Lect. Notes Comput. Sci., G. Fichtinger, A. Martel, and T. Peters, Eds., vol. 6893. Springer, 2011, pp. 330–337.

[14] A. Charnoz, V. Agnus, G. Malandain, L. Soler, and M. Tajine, "Tree matching applied to vascular system," in *Proc. IAPR Int. Conf. on Graph-based Represent. (GbRPR)*, ser. Lect. Notes Comput. Sci., L. Brun and M. Vento, Eds., vol. 3434. Springer, 2005, pp. 183–192.

[15] J. N. Kaftan, "A novel multipurpose tree and path matching algorithm with application to airway trees," in *Proc. SPIE Med. Imag.*, A. Manduca and A. A. Amini, Eds., vol. 6143. SPIE Press, 2006, pp. 215–224, article 61430N.

[16] J. H. Metzen, T. Kröger, A. Schenk, S. Zidowitz, H.-O. Peitgen, and X. Jiang, "Matching of anatomical tree structures for registration of medical images," *Image Vis. Comput.*, vol. 27, no. 7, pp. 923–933, Jun. 2009.

[17] C. Oyarzun Laura and K. Drechsler, "Computer assisted matching of anatomical vessel trees," *Comput. Graph.*, vol. 35, no. 2, pp. 299–311, Apr. 2011.

[18] T. Lohe, T. Kroger, S. Zidowitz, H. Peitgen, and X. Jiang, "Hierarchical matching of anatomical trees for medical image registration," in *Proc. Int. Conf. Med. Biom.*, ser. Lect. Notes Comput. Sci., vol. 4901. Springer, 2007, pp. 224–231.

[19] M. W. Graham and W. E. Higgins, "Optimal graph-theoretic approach to 3D anatomical tree matching," in *Proc. IEEE Int. Symp. Biomed. Imag. (ISBI)*. IEEE Press, 2006, pp. 109–112.

[20] D. Smeets, P. Bruyninckx, J. Keustermans, D. Vandermeulen, and P. Suetens, "Robust matching of 3D lung vessel trees," in *Int. Workshop on Pulm. Image Anal.*, 2010, pp. 61–70.

[21] T. Bülow, C. Lorenz, R. Wiemker, and J. Honko, "Point based methods for automatic bronchial tree matching and labeling," in *Proc. SPIE Med. Imag.*, A. Manduca and A. A. Amini, Eds., vol. 6143. SPIE Press, 2006, article 61430O.

[22] A. Feragen, J. Petersen, M. Owen, P. Lo, L. H. Thomsen, M. M. W. Wille, A. Dirksen, and M. de Bruijne, "A hierarchical scheme for geodesic anatomical labeling of airway trees," in *Proc. Int. Conf. Med. Imag. Comput. & Comput. Assist. Interven. (MICCAI)*, ser. Lect. Notes Comput. Sci., N. Ayache, H. Delingette, P. Golland, and K. Mori, Eds., vol. 7512. Springer, 2012, pp. 147–155.

[23] M. W. Graham, "Robust graph-theoretic methods for matching and labeling anatomical trees," Ph.D. dissertation, The Pennsylvania State University, 2006.

[24] J. Tschirren, G. McLennan, K. Palagyi, E. A. Hoffman, and M. Sonka, "Matching and anatomical labeling of human airway tree," *IEEE Trans. Med. Imag.*, vol. 24, no. 12, pp. 1540–1547, Dec. 2005.

[25] B. van Ginneken, W. Baggerman, and E. M. van Rikxoort, "Robust segmentation and anatomical labeling of the airway tree from thoracic CT scans," in *Proc. Int. Conf. Med. Imag. Comput. & Comput. Assist. Interven. (MICCAI)*, ser. Lect. Notes Comput. Sci., D. Metaxas, L. Axel,

G. Fichtinger, and G. Szekely, Eds., vol. 5241. Springer, 2008, pp. 219–226.

[26] K. Mori, J. Hasegawa, Y. Suenaga, and J. Toriwaki, "Automated anatomical labeling of the bronchial branch and its application to the virtual bronchoscopy system," *IEEE Trans. Med. Imag.*, vol. 19, no. 2, pp. 103–114, Feb. 2000.

[27] S. Ota, D. Deguchi, T. Kitasaka, K. Mori, Y. Suenaga, Y. Hasegawa, K. Imaizumi, H. Takabatake, M. Mori, and H. Natori, "Augmented display of anatomical names of bronchial branches for bronchoscopy assistance," in *Proc. Med. Imag. Augment. Reality (MIAR)*, ser. Lect. Notes Comput. Sci., T. Dohi, I. Sakuma, and H. Liao, Eds., vol. 5128. Springer, 2008, pp. 377–384.

[28] K. Mori, S. Ota, D. Deguchi, T. Kitasaka, Y. Suenaga, S. Iwano, Y. Hasegawa, H. Takabatake, M. Mori, and H. Natori, "Automated anatomical labeling of bronchial branches extracted from CT datasets based on machine learning and combination optimization and its application to bronchoscope guidance." in *Proc. Int. Conf. Med. Imag. Comput. & Comput. Assist. Interven. (MICCAI)*, ser. Lect. Notes Comput. Sci., G.-Z. Yang, D. Hawkes, D. Rueckert, A. Noble, and C. Taylor, Eds., vol. 5762. Springer, 2009, pp. 707–714.

[29] K. Haris, S. N. Efstratiadis, N. Maglaveras, C. Pappas, J. Gourassas, and G. Louridas, "Model-based morphological segmentation and labeling of coronary angiograms," *IEEE Trans. Med. Imag.*, vol. 18, no. 10, pp. 1003–1015, Oct. 1999.

[30] C. Chalopin, G. Finet, and I. E. Magnin, "Modeling the 3D coronary tree for labeling purposes," *Med. Image Anal.*, vol. 5, pp. 301–315, Dec. 2001.

[31] K. Mori, M. Oda, T. Egusa, Z. Jiang, T. Kitasaka, M. Fujiwara, and K. Misawa, "Automated nomenclature of upper abdominal arteries for displaying anatomical names on virtual laparoscopic images," in *Proc. Med. Imag. Augment. Reality (MIAR)*, ser. Lect. Notes Comput. Sci., H. Liao, E. Edwards, X. Pan, Y. Fan, and G.-Z. Yang, Eds., vol. 6326. Springer, 2010, pp. 353–362.

[32] W. Tang and A. Chung, "Cerebral vascular tree matching of 3D-RA data based on tree edit distance," in *Proc. Med. Imag. Augment. Reality (MIAR)*, ser. Lect. Notes Comput. Sci., G.-Z. Yang, T. Jiang, D. Shen, L. Gu, and J. Yang, Eds., vol. 4091. Springer, 2006, pp. 116–123.

[33] Y. Uchiyama, M. Yamauchi, H. Ando, R. Yokoyama, T. Hara, H. Fujita, T. Iwama, and H. Hoshi, "Automated classification of cerebral arteries in MRA images and its application to maximum intensity projection," in *Proc. Int. Conf. IEEE Eng. Med. Biol. Soc. (EMBC)*. IEEE press, 2006, pp. 4865–4868.

[34] I. Volkau, W. Zheng, R. Baimouratov, A. Aziz, and W. L. Nowinski, "Geometric modeling of the human normal cerebral arterial system," *IEEE Trans. Med. Imag.*, vol. 24, no. 4, pp. 529–539, Apr. 2005.

[35] C. Kirbas and F. Quek, "A review of vessel extraction techniques and algorithms," *ACM Comput. Surv.*, vol. 36, pp. 81–121, Jun. 2004.

[36] D. Lesage, E. D. Angelini, I. Bloch, and G. Funka-Lea, "A review of 3D vessel lumen segmentation techniques: Models, features and extraction schemes," *Med. Image Anal.*, vol. 13, no. 6, pp. 819 – 845, Dec. 2009.

[37] S. R. Aylward and E. Bullitt, "Initialization, noise, singularities, and scale in height ridge traversal for tubular object centerline extraction," *IEEE Trans. Med. Imag.*, vol. 21, no. 2, pp. 61–75, Feb. 2002.

[38] "TubeTK: Segmentation, registration, and analysis of tubular structures in images," http://public.kitware.com/Wiki/TubeTK, 2012.

[39] R. Cardenes, J. L. Diez, H. Bogunovic, I. Larrabide, and A. F. Frangi, "3D modeling coronary artery bifurcations from CTA and conventional coronary angiography," in *Proc. Int. Conf. Med. Imag. Comput. & Comput. Assist. Interven. (MICCAI)*, ser. Lect. Notes Comput. Sci., G. Fichtinger, A. Martel, and T. Peters, Eds., vol. 6893. Springer, 2011, pp. 395–402.

[40] M. Hernandez and A. F. Frangi, "Non-parametric geodesic active regions: method and evaluation for cerebral aneurysms segmentation in 3DRA and CTA," *Med. Image Anal.*, vol. 11, no. 3, pp. 224–241, Jun. 2007.

[41] H. Bogunovic, J. M. Pozo, M. C. Villa-Uriol, C. B. L. M. Majoie, R. van den Berg, H. A. F. Gratama van Andel, J. M. Macho, J. Blasco, L. San Roman, and A. F. Frangi, "Automated segmentation of cerebral vasculature with aneurysms in 3DRA and TOF-MRA using geodesic active regions: An evaluation study," *Med. Phys.*, vol. 38, pp. 210–222, Jan. 2011.

[42] X. Han, C. Xu, and J. L. Prince, "A topology preserving level set method for geometric deformable models," *IEEE Trans. Pattern Anal. Mach. Intell.*, vol. 25, no. 6, pp. 755–768, Jun. 2003.

[43] L. Antiga and D. A. Steinman, "Robust and objective decomposition and mapping of bifurcating vessels." *IEEE Trans. Med. Imag.*, vol. 23, no. 6, pp. 704–713, Jun. 2004.

[44] M. Piccinelli, A. Veneziani, D. A. Steinman, A. Remuzzi, and L. Antiga, "A framework for geometric analysis of vascular structures: application to cerebral aneurysms." *IEEE Trans. Med. Imag.*, vol. 28, no. 8, pp. 1141–1155, Aug. 2009.

[45] L. Antiga and D. A. Steinman, "VMTK: the Vascular Modeling Toolkit," http://www.vmtk.org, 2012.

[46] P. T. Fletcher, C. Lu, S. M. Pizer, and S. Joshi, "Principal geodesic analysis for the study of nonlinear statistics of shape," *IEEE Trans. Med. Imag.*, vol. 23, no. 8, pp. 995–1005, Aug. 2004.

[47] D. H. Ballard and C. M. Brown, *Computer Vision*. Prentice Hall, 1982.

[48] M. Pelillo, K. Siddiqi, and S. W. Zucker, "Matching hierarchical structures using association graphs," *IEEE Trans. Pattern Anal. Mach. Intell.*, vol. 21, no. 11, pp. 1105–1120, Nov. 1999.

[49] I. M. Bomze, M. Budinich, P. M. Pardalos, and M. Pelillo, "The maximum clique problem," in *Handbook of Combinatorial Optimization*, D.-Z. Du and P. M. Pardalos, Eds. Kluwer Academic, 1999, vol. 4, pp. 1–74.

[50] E. Tomita, A. Tanaka, and H. Takahashi, "The worst-case time complexity for generating all maximal cliques and computational experiments," *Theor. Comput. Sci.*, vol. 363, no. 1, pp. 28–42, Oct. 2006.

[51] E. Bullitt, D. Zeng, G. Gerig, S. Aylward, S. Joshi, J. K. Smith, W. Lin, and M. G. Ewend, "Vessel tortuosity and brain tumor malignancy: A blinded study," *Acad. Radiol.*, vol. 12, no. 10, pp. 1232–1240, Oct. 2005.

[52] H. Bogunovic, J. M. Pozo, R. Cardenes, and A. F. Frangi, "Automatic identification of internal carotid artery from 3DRA images," in *Proc. Int. Conf. IEEE Eng. Med. Biol. Soc. (EMBC)*. IEEE Press, 2010, pp. 5343–5346.

[53] N. Tanriover, M. Kawashima, A. L. Rhoton, A. J. Ulm, and R. A. Mericle, "Microsurgical anatomy of the early branches of the middle cerebral artery: morphometric analysis and classification with angiographic correlation," *J. Neurosurg.*, vol. 98, no. 6, pp. 1277–1290, Jun. 2003.

[54] A. J. Ulm, G. L. Fautheree, N. Tanriover, A. Russo, E. Albanese, A. L. Rhoton, R. A. Mericle, and S. B. Lewis, "Microsurgical and angiographic anatomy of middle cerebral artery aneurysms: prevalence and significance of early branch aneurysms," *Neurosurgery*, vol. 62, no. 5 Suppl 2, pp. 344–352, May 2008.

[55] S. M. Pizer, P. T. Fletcher, S. Joshi, A. Thall, J. Z. Chen, Y. Fridman, D. S. Fritsch, A. G. Gash, J. M. Glotzer, M. R. Jiroutek, C. Lu, K. E. Muller, G. Tracton, P. Yushkevich, and E. L. Chaney, "Deformable M-Reps for 3D medical image segmentation," *Int. J. Comput. Vis.*, vol. 55, no. 2-3, pp. 85–106, Nov. 2003.

[56] K. Siddiqi and S. Pizer, *Medial Representations: Mathematics, Algorithms and Applications*. Springer, 2008.

[57] H. Bogunovic, J. M. Pozo, R. Cardenes, M. C. Villa-Uriol, R. Blanc, M. Piotin, and A. F. Frangi, "Automated landmarking and geometric characterization of the carotid siphon," *Med. Image Anal.*, vol. 16, no. 4, pp. 889–903, May 2012.